Combined Phase-Readout and Self-Calibration of MEMS Gyroscopes

A. N. Shirazi, G. Casinovi, M. Dalal and F. Ayazi

16th International Conference on Solid-State Sensors, Actuators and Microsystems (TRANSDUCERS)
pp. 960–963, June 2013

Abstract

This paper presents a gyroscope interface architecture that combines readout and self-calibration functions in a reconfigurable fashion. The phase readout and calibration operation relies on the phase shifts observed at the gyroscope outputs with respect to the applied excitations. The proposed electrostatic calibration obviates the use of any additional moving parts or calibration stage. The significance of this work is having shared interface electronics between the readout and calibration configurations, which inherently compensates for the sources of drift in the electronics, resulting in improved calibration accuracy. Experimental data is presented that supports the theoretical analysis of the proposed readout and self-calibration schemes.

Copyright Notice

COMBINED PHASE-READOUT AND SELF-CALIBRATION OF MEMS GYROSCOPES

A. N. Shirazi, G. Casinovi, M. Dalal, and F. Ayazi
Georgia Institute of Technology, Atlanta, Georgia, USA

ABSTRACT

This paper presents a gyroscope interface architecture that combines readout and self-calibration functions in a reconfigurable fashion. The phase readout and calibration operation relies on the phase shifts observed at the gyroscope outputs with respect to the applied excitations. The proposed electrostatic calibration obviates the use of any additional moving parts or calibration stage. The significance of this work is having shared interface electronics between the readout and calibration configurations, which inherently compensates for the sources of drift in the electronics, resulting in improved calibration accuracy. Experimental data is presented that supports the theoretical analysis of the proposed readout and self-calibration schemes.

KEYWORDS

MEMS gyroscope, self-calibration, phase readout, mode misalignment, high frequency gyroscope

INTRODUCTION

The use of MEMS inertial sensors has become widespread in many consumer products [1], [2]. Considerable research is now directed towards improving their performance to levels that would make them suitable for use in more demanding applications, such as GPS augmentation systems. The development of effective self-calibration techniques would mark a significant step in that direction, because they would make it possible to maintain high accuracy in the sensors over time without the need for periodic off-line recalibration in specialized facilities.

This paper presents a combined readout and self-calibration architecture for MEMS resonant gyroscopes that does not require the use of any additional moving parts or calibration stage. The principle of operation of this architecture is based on the observation that the Coriolis force induces a phase-shift between the gyroscope inputs and its outputs, and that a similar phase-shift also occurs when the gyroscope is subjected to an excitation that rotates in the 2-DOF reference system created by an abstract mass-spring model of the gyroscope. It is shown that a simple mathematical relationship exists between the phase-shift induced by the Coriolis force and that created by a rotating excitation [3]. Therefore the gyroscope can be calibrated by mimicking the effect of the Coriolis force through the application of a rotating excitation to the device, which can be achieved without having to physically move the device (e.g. through suitable amplitude-modulated inputs). Therefore this technique would completely eliminate the need for any mechanical calibration of MEMS gyroscopes, with clear advantages in terms of system stability, reliability and cost-effectiveness.

A practical realization of a gyroscope readout scheme that relies on the Coriolis-induced phase-shift has already been demonstrated [4]. In this paper it is shown that phase-based readout and calibration functions can be integrated in a reconfigurable fashion, so that processing of the gyroscope outputs is performed by the same electronics in both cases. This means that any changes in those electronics due to aging or other environmental factors will affect readout and calibration outputs equally, thus increasing the accuracy of the calibration of the device.

GYROSCOPE MODES OF OPERATION

The readout and calibration schemes described in this paper are based on the well-known equivalent 2-DOF mass-spring model of a gyroscope. Neglecting the centrifugal forces and assuming that the frequencies of the two resonance modes of the gyroscope coincide, this model is represented mathematically by the following equations:

$$\begin{aligned} \ddot{x}_1 + \frac{\omega_0}{Q}\dot{x}_1 - 2\lambda\Omega_z\dot{x}_2 + \omega_0^2 x_1 &= f_1(t) \\ \ddot{x}_2 + \frac{\omega_0}{Q}\dot{x}_2 + 2\lambda\Omega_z\dot{x}_1 + \omega_0^2 x_2 &= f_2(t) \end{aligned} \qquad (1)$$

where x_1, x_2 are generalized normal-mode coordinates, ω_0 the frequency of the two degenerate resonance modes of the gyroscope, Q their quality factor, Ω_z the angular velocity of rotation of the gyroscope around its sensitive axis, and λ a constant that depends on the gyroscope type and on the index of the resonance modes of the device [5]. This model is used to analyze the behavior of the gyroscope in readout and calibration modes.

Readout Mode

Operation of the gyroscope in readout mode is attained by setting $f_1(t) = F_1\cos\omega_0 t$, $f_2(t) = F_2\sin\omega_0 t$. It has been shown in [4] that the steady-state response of (1) to these excitations is

$$x_1(t) = \frac{Q}{\omega_0}\frac{\sqrt{(F_1\omega_0)^2 + (2F_2Q\lambda\Omega_z)^2}}{\omega_0^2 + (2Q\lambda\Omega_z)^2}\sin(\omega_0 t - \theta_1)$$

$$x_2(t) = -\frac{Q}{\omega_0}\frac{\sqrt{(F_2\omega_0)^2 + (2F_1Q\lambda\Omega_z)^2}}{\omega_0^2 + (2Q\lambda\Omega_z)^2}\cos(\omega_0 t - \theta_2)$$

where

$$\theta_1 = \tan^{-1}\frac{2F_2Q\lambda\Omega_z}{F_1\omega_0}, \quad \theta_2 = \tan^{-1}\frac{2F_1Q\lambda\Omega_z}{F_2\omega_0}.$$

The equations above show that θ_1 and θ_2, which represent phase-shifts in the gyroscope output signals, are directly related to Ω_z. Signals proportional to those phase shifts can be obtained by standard synchronous phase

demodulation circuits, consisting of mixers that generate $w_1(t)=x_1(t)F_1\cos\omega_0 t$, and $w_2(t)=x_2(t)F_2\sin\omega_0 t$, followed by low-pass filters. The outputs of the filters, z_1 and z_2, are the DC components of $w_1(t)$ and $w_2(t)$, respectively. It can be shown that they are the same and that they are given by the following expression

$$z_1 = z_2 = -\frac{QF_1F_2}{2\omega_0^2} f\left(\lambda\frac{2\Omega_z}{\omega_0/Q}\right) \qquad (2)$$

where $f(x) = x/(x^2+1)$. This relationship shows that z_1 and z_2 can be used to measure the rotation rate of the gyroscope around its sensitive axis.

Calibration Mode

When the gyroscope is operating in calibration mode, its inputs are amplitude modulated, so as to create an excitation that rotates in the plane of the mass-spring model coordinates [3]. Then the governing equations (1) become

$$\begin{aligned}\ddot{x}_1 + \frac{\omega_0}{Q}\dot{x}_1 + \omega_0^2 x_1 &= F_1\cos\omega_0 t\cos\Omega_z t \\ \ddot{x}_2 + \frac{\omega_0}{Q}\dot{x}_2 + \omega_0^2 x_2 &= F_2\sin\omega_0 t\sin\Omega_z t\end{aligned} \qquad (3)$$

Note that in this case the dynamics of the two modes are decoupled, because it is assumed that the gyroscope is stationary during calibration. The steady-state solution to (3) can be obtained from standard frequency-domain analysis. However, for brevity, only a summary of the main results is provided here.

Let

$$H(j\omega) = -\omega^2 + j\omega(\omega_0/Q) + \omega_0^2$$

Then the steady-state solution to the first equation in (3) is

$$\begin{aligned}x_1(t) = &\frac{F_1}{2H_+}\cos[(\omega_0+\Omega_z)t-\theta_+] \\ &+\frac{F_1}{2H_-}\cos[(\omega_0-\Omega_z)t-\theta_-]\end{aligned}$$

where

$$\begin{aligned}H_+ &= \left|H[j(\omega_0+\Omega_z)]\right| \quad \theta_+ = \angle H[j(\omega_0+\Omega_z)] \\ H_- &= \left|H[j(\omega_0-\Omega_z)]\right| \quad \theta_- = \angle H[j(\omega_0-\Omega_z)]\end{aligned}$$

Mixing $x_1(t)$ with the excitation to $x_2(t)$, and vice versa, yields

$$\begin{aligned}w_1(t) &= x_1(t)F_2\sin\omega_0 t\sin\Omega_z t \\ w_2(t) &= x_2(t)F_1\cos\omega_0 t\cos\Omega_z t\end{aligned}$$

As in readout mode, the DC components of $w_1(t)$ and $w_2(t)$ are eliminated by low-pass filtering. The resulting outputs are

$$z_1 = z_2 = \frac{1}{2}\frac{QF_1F_2}{2\omega_0^2} f\left(\frac{2\Omega_z}{\omega_0/Q}\right) \qquad (4)$$

where $f(x) = x/(x^2+1)$, as before.

A comparison of (2) and (4) leads to the following conclusion: When the gyroscope is operating in readout mode and rotating at angular velocity Ω_z, the values of the final outputs are twice those generated when the gyroscope is operating in calibration mode with a "virtual rotation rate" $\lambda\Omega_z$.

If $\Omega_z << \omega_0/Q$, then $x << 1$ and $f(x) \cong x$. In this case, the values of the final output signals are proportional to Ω_z, and the scale factor of the architecture in readout mode is 2λ times its scale factor in calibration mode.

Mode Mismatches

In most practical instances, the two resonance modes of the gyroscope are not exactly identical. If calibration has to be performed with a high degree of accuracy, the effect of mode mismatches on gyroscope operation must be accounted for.

A fully general analysis of the behavior of a gyroscope with mismatched modes is impracticably complex. However, the difference in the resonance frequencies of the two modes is usually the dominant effect. In such case a simpler analysis can be performed under the additional assumption that Ω_z is small enough for the gyroscope response to be linear. This assumption is justified in most practical cases, especially if the gyroscope resonance frequencies are in the Megahertz range.

Let ω_1 and ω_2 be the frequencies of the resonance modes of the gyroscope, and let ω_0 be the frequency of the applied excitation. Assume that the gyroscope outputs are processed as described earlier in this section, and also assume that the quality factor of both modes are identical and equal to Q. Then the analysis, the details of which are omitted for space reasons, yields the following expression for the scale factor of the readout architecture:

$$\begin{aligned}SF_{read} = &\frac{\lambda F_1F_2}{\omega_0}\times \\ &\frac{4\Delta\omega_1\Delta\omega_2 - (\omega_0/Q)^2}{[(2\Delta\omega_1)^2+(\omega_0/Q)^2][(2\Delta\omega_2)^2+(\omega_0/Q)^2]}\end{aligned} \qquad (5)$$

where $\Delta\omega_1 = \omega_1 - \omega_0$, $\Delta\omega_2 = \omega_2 - \omega_0$. In particular, the scale factor is the same for both outputs.

On the other hand, the resonance modes of the gyroscope are decoupled in calibration operation. Consequently, the calibration scale factors of the two outputs are generally different. Specifically, it can be shown that the scale factor at the first output is given by:

$$SF_{cal1} = \frac{F_1F_2}{2\omega_0}\frac{(\omega_0/Q)^2 - (2\Delta\omega_1)^2}{\left[(2\Delta\omega_1)^2+(\omega_0/Q)^2\right]^2}. \qquad (6)$$

The calibration scale factor at the other output is obtained by substituting $\Delta\omega_2$ for $\Delta\omega_1$ in the expression above.

INTERFACE CIRCUIT ARCHITECTURE

The block diagram of a reconfigurable system architecture that combines the phase-readout and self-calibration techniques described in the previous sections is shown in Fig. 1. The mathematical representation of the system operation is also shown.

The input excitations described in (1) and (3) are provided by an AM I/Q signal generator consisting of two mixers and two 90° phase-shifters. On each mixer, one input is at carrier frequency ω_0, while the other input is either at DC in the readout mode ($A(t)$ = DC), or at Ω_Z for self-calibration ($A(t) = \cos\Omega_z t$).

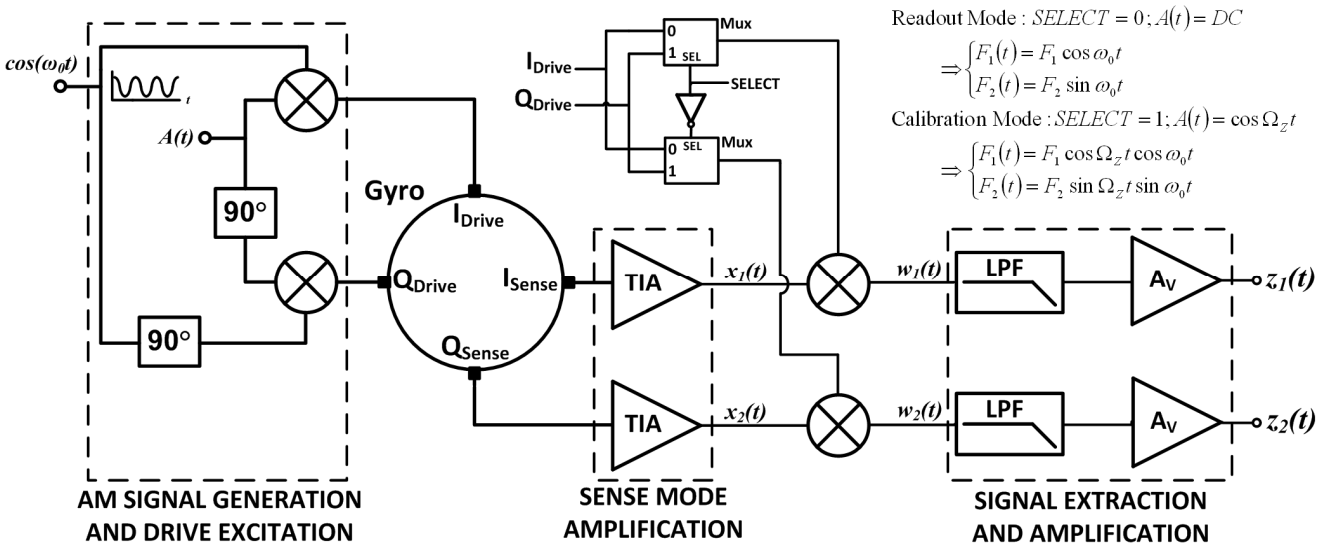

Figure 1: System-level block diagram of the combined self-calibration and phase-readout architecture. The gyroscope is actuated at both its drive and sense resonance modes, in both configurations.

At the output of the gyroscope, two transimpedance amplifiers (TIA) are used to translate the output currents into voltages. Two analog multiplexers are used to connect the right combination of drive signals to the demodulating mixers.

In readout mode SELECT is set to logic 0, and therefore the output of each mode is mixed to its respective input, e.g. I_{SENSE} is mixed with I_{DRIVE}. In self-calibration mode SELECT is set to logic 1, and therefore the output of each mode is mixed with the input of the other mode, e.g. I_{SENSE} is mixed with Q_{DRIVE}. The signals $w_1(t)$ and $w_2(t)$ are then low-pass filtered to generate $z_1(t)$ and $z_2(t)$ outputs.

The PCB implementation of the reconfigurable system is shown in Fig. 2.

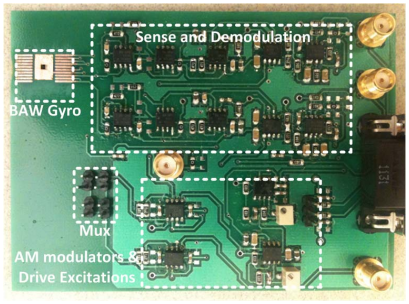

Figure 2: *PCB implementation of the reconfigurable phase-readout and self-calibration architecture.*

The sense path and I/Q demodulator section consist of sense TIAs followed by multiplier ICs, low-pass filters and rate amplifiers. TI OPA657 opamps have been used for all the amplifiers, including high-frequency TIAs and gain-stages. AD835 multipliers from Analog Devices are used for demodulation. The multiplier output is filtered by a 2nd-order Butterworth low-pass Sallen-key filter implemented by Analog Devices AD8639 dual-opamps. The second opamp in the IC is used for rate amplification, followed by another 1st-order RC low-pass filter.

Discrete jumpers are used for analog multiplexing at the input of the mixers. Using these jumpers, the operation mode can be switched to readout mode or calibration mode at any time.

The AM signal generation includes two AD835 multiplier ICs, mixing the external carrier frequency (ω_0) signal with the modulation signal $A(t)$. In order to generate I/Q carrier signals at ω_0, an all-pass phase-shifter is used to convert $\cos\omega_0 t$ provided by signal generator, into $\sin\omega_0 t$, while the I/Q calibration excitations are individually provided by an external dual-output function generator, for more convenience.

A high-frequency bulk acoustic wave (BAW) disk gyroscope [6], [7], has been used in this experiment. Fig. 3a shows the SEM view and the die photo of the wafer-level packaged BAW gyroscope. As shown in Fig. 3b, the drive mode of the 600 µm diameter disk gyroscope has a quality factor of 55,000 at 9.64 MHz. The two degenerate n = 3 modes of the BAW disk gyroscope are shown in Fig. 3c.

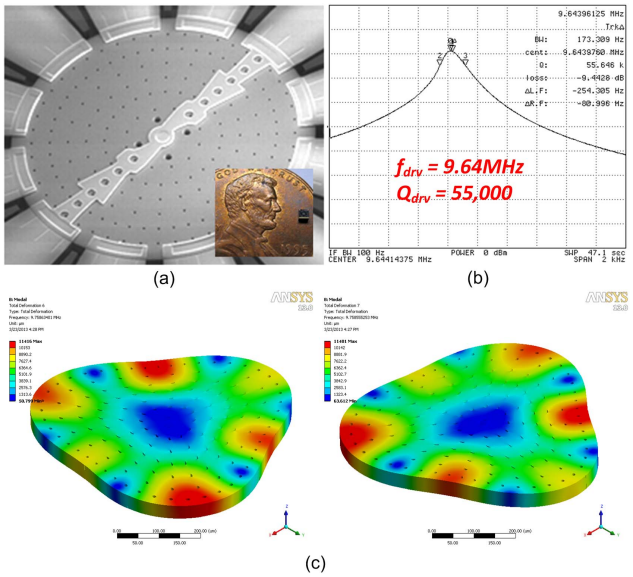

Figure 3: (a) SEM picture and die image (wafer level packaged die) of the high-frequency BAW disk gyroscope, (b) Drive mode of the BAW gyroscope showing a high Q of 55,000 at 9.64 MHz (c) Simulation results showing two degenerate n=3 modes of the gyroscope at 9.75 MHz.

MEASUREMENT RESULTS

In readout mode, as shown in Fig. 4, a physical scale factor of 115 µV/°/sec has been measured at 0dBm input power, for input rotation rates from 1 to 20 °/sec.

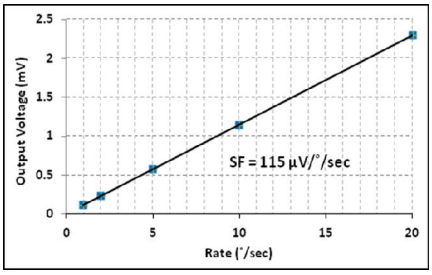

Figure 4: A physical scale factor of 115 µV/°/sec is measured from the readout configuration at 0 dBm input power.

In calibration mode, the calibration scale factor was measured at 0 dBm input power, while the rotating excitation amplitude is equal to the DC voltage applied in readout mode. As can be seen in Fig. 5a, the frequency of the electrostatic rate is changed from 10 Hz to 15 Hz in 1 Hz steps, every few seconds, to mimic rotation rates from 3600 °/sec to 5400 °/sec in 360 °/sec steps.

The acquired data points in the staircase are put together in Fig. 5b to show a sensitivity of 26.3 mV/Hz, which translates into 73 µV/°/sec calibration scale factor, when divided by 360° rotation angle.

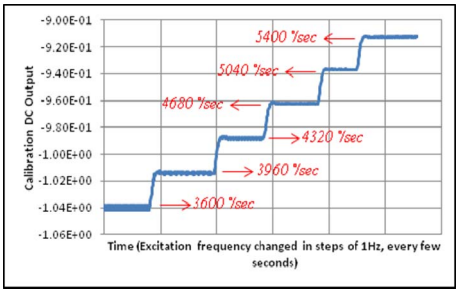

(a)

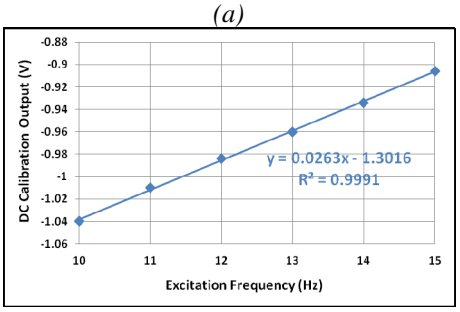

(b)

Figure 5: (a) The excitation frequency is changed from 10 Hz to 15 Hz (equivalently 3600 °/sec to 5400 °/sec) in 1Hz (360°/sec) steps every few seconds, (b) A scale factor of 26.3 mV/Hz (73 µV/°/sec) has been measured for the calibration configuration.

In order to match the physical and calibration scale factors in presence of mode frequency mismatches, the measured scale factor values must be readjusted by the calculated values from (5) and (6).

Considering that the drive-mode of the gyroscope shows a quality factor of 55,000 at 9.64 MHz resonance frequency, and accounting for 250 Hz split between the frequencies of the two modes, a ratio of 1.53 can be calculated for the ratio of the scale factor in readout mode, SF_{read}, over the calibration scale factor, SF_{cal1}.

When readjusted by mathematical analysis, the measured calibration scale factor corresponds to 111.7 µV/°/sec estimated scale factor in readout mode, which shows good agreement with the actual measurement result shown in Fig.4. The 3% matching error between the estimated and actual scale factors is due to inaccuracies in the measurement setup.

CONCLUSION

A complete mathematical analysis of phase-readout and self-calibration techniques, accounting for the effect of mode frequency mismatches was presented. A combined reconfigurable phase-readout and self-calibration system was implemented and measured. Mathematical calculations show that the results obtained from calibration measurements can be used to predict the physical scale factor of the readout configuration.

ACKNOWLEDGEMENTS

The authors wish to thank DARPA for supporting this work under the PASCAL program, contract #W31P4Q-12-1-0004. This project was also funded in part by Qualtré.

REFERENCES

[1] B. Vigna, "It Makes Sense: How Extreme Analog and Sensing Will Change the World," in *Tech. Digest 2012 Solid-State Sensors, Actuators and Microsystems Workshop*, Hilton Head, SC, June 2012, pp. 58–65.

[2] F. Ayazi, "Multi-DOF Inertial MEMS: From Gaming to Dead Reckoning," in *Digest Tech. Papers Transducers'11 Conference*, Beijing, China, June 2011, pp 2805-2808.

[3] G. Casinovi, W. K. Sung, M. Dalal, A. N. Shirazi, and F. Ayazi, "Electrostatic Self-Calibration of Vibratory Gyroscopes," in *Proc. 25th IEEE Int. Conference on Micro Electro Mechanical Systems*, Paris, France, Jan. 2012, pp. 559–562.

[4] M. Dalal, A. N. Shirazi, W. K. Sung, G. Casinovi, and F. Ayazi, "Novel Readout Scheme for MEMS Vibratory Gyroscopes Based on Signal Phase Shift," in *Tech. Digest 2012 Solid-State Sensors, Actuators and Microsystems Workshop*, Hilton Head, SC, June 2012, pp. 328–331.

[5] B. J. Gallacher *et al*, "Principles of a Three-Axis Vibrating Gyroscope", *IEEE Trans. Aerosp. Electron. Syst.*, vol. 37, pp. 1333–1343, 2001.

[6] http://www.qualtre.com

[7] H. Johari, and F. Ayazi, "Capacitive Bulk Acoustic Wave Silicon Disk Gyroscopes," in *Tech. Digest 2006 IEEE Intl. Electron Devices Meeting (IEDM 2006),* San Francisco, CA, Dec. 2006, pp. 513-516.

CONTACT

A.N. Shirazi, tel: +1-404-385-6693; arashk.n@gatech.edu